Helix Distortion and Crystal Structure of the α-Form of Poly(L-lactide)

S. Sasaki* and T. Asakura

Japan Advanced Institute of Science and Technology, 1-1 Asahidai, Tatsunokuchi, Ishikawa 923-1292, Japan

Received June 26, 2003; Revised Manuscript Received September 2, 2003

ABSTRACT: The crystal structure of the α-form of poly(L-lactide) was analyzed by the linked-atom least-squares refinements for the X-ray fiber diffraction data. The space group was orthorhombic $P2_12_12_1$, and the unit cell contained the antiparallel two chains. The chain conformation was the 2-fold s(15*2/7) helix distorted periodically from the regular s(3*10/7) helix. The ester groups were deformed from the planar trans conformation. Potential energy calculations suggested that the periodic chain distortion resulted from the impartial stress distribution due to the interchain interactions.

Introduction

Poly(L-lactide) (PLLA), $-[-OCH(CH_3)CO-]_n-$, is a chiral polyester analogue of poly(L-alanine) and can be processed to high-strength fibers. Many applications have been developed for the biodegradable and biocompatible properties. The molecular and crystal structure has been studied mainly by means of potential energy calculations and diffraction methods.[1−14] Depending on the preparation condition, PLLA crystallizes in three modifications (α-, *β*-, and *γ*-forms). The *β*-form is prepared at high draw ratio and high drawing temperature. The chain conformation is the left-handed 3-fold helix[4,5,10] and has been described as left-handed 3/1, −3/1, 3/2, left-handed 3_1, or 3_2. If we conform to the conventional *M*/*N* notation where the integer *M* denotes the number of residues contained in *N* helical turns, the notation 3/2 is unequivocal, where the unit twist and the unit height are explicitly defined to be $2\pi N/M$ and c/M, respectively (c is the axial translation distance). In the IUPAC notation of s(*A***M*/*N*),[15] where the helix class *A* identifies the number of skeletal atoms contained in the helix residue, the conformation of the *β*-form is described to be s(3*3/2). It is recommended that the index *A* can be dropped if deemed unnecessary and the expression is simply equivalent to *M*/*N*, but the index *A* is meaningful under some circumstances as is mentioned below. The notation M_N, however, is ambiguous. This type of notation has expressed the crystallographic *M*-fold screw axis, which is defined by the right-handed screw rotation of 360/*M* degrees around an axis coupled with screw pitch $(N/M)c$.[16] The crystallographic M_N helix is not always equivalent to s(*M*/*N*). Actually, s(3/2) is 3_2, whereas s(10/7), the essential conformation of the α-form, is 10_3. In the present work we address the IUPAC notation in order to avoid the confusion. The chain packing in the *β*-form has recently been explained in terms of a frustrated structure.[10] The *γ*-form[9] found by the epitaxial crystallization contains two antiparallel s(3/2) helices in the pseudoorthorhombic unit cell.

The stable α-form exhibits the well-defined fiber diffraction pattern.[5] From the potential energy calculations and the diffractions, the chain conformation was determined to be s(3*10/7).[2,5,6,12] The unit cell is rectangular with dimensions $a \approx 10.7$ Å, $b \approx 6.2$ Å, and c (chain axis) ≈ 28.8 Å, but the space group has not been established yet. The unit cell contains two chains that are considered to be antiparallel. The regularity in the arrangement of the up- and down-pointing chains should influence the structure. The s(10/7) and s(3/2) helices assume very similar conformation and have approximately the same energy. Hoogsteen et al.[5] pointed out that despite the close resemblance the transformation between the α- and *β*-forms was hard to obtain. Since the rearrangement of the up- and down-pointing chains hardly takes place in the solid state, their packing must be responsible for the polymorphism.

For the regular s(3*10/7) structure, the meridional reflections should appear only on every 10 layer lines. De Santis and Kovacs[2] found the extra meridional reflections on the layer lines with the number $l = 2$, 6, 7, 8, and 9, and Hoogsteen et al.[5] observed those on $l = 2$, 4, 6, 7, 8, and 9, while Kobayashi et al.[6] reported on $l = 3$, 4, 6, 7, 8, and 18. The inconsistency may be due to the difference in the manner of up−down chain arrangements in their specimens. The conformation is certainly distorted periodically from the regular helix owing to the interchain interactions.[5] This kind of periodic distortion has often been observed in polymer crystals.[17−20] The chain of poly(L-alanine), for instance, takes the stiff α-helix conformation, but some extra meridional reflections are clear evidence for the distortion.[17] The chain of poly(ethylene oxide) is rather flexible and suffers from the considerable distortion from the s(3*7/2) helix.[18] Since the symmetry cannot be suited to any crystallographic lattice symmetry, the seven monomeric units (21 backbone atoms) form an asymmetric unit, namely s(21*1/2). In the case of the α-form of PLLA, only the 2-fold screw axis, which is an element of the molecular group s(3*10/7), is suitable for the lattice symmetry. Therefore, the helix will be distorted at least to the 2-fold s(15*2/7) helix, where five monomeric units (15 backbone atoms) form an asymmetric unit. For this model, meridional reflections should not appear on the odd layer lines. The very weak 003 and 007 reflections are considered to be attributable to the disordered packing.

Kobayashi et al.[6] proposed the pseudoorthorhombic (triclinic) unit cell for the α-form, in which two chains with the same direction were arranged at uneven intervals. The packing did not seem reasonable, and the agreement between the observed and calculated intensi-

* Corresponding author. E-mail: s-sasaki@jaist.ac.jp.

10.1021/ma0348674 CCC: $25.00
Published on Web 10/04/2003

ties was poor. For the rectangular unit cell, we must investigate orthorhombic space groups. Because of the chain chirality, the space group can possess neither centrosymmetry nor glide planes. The symmetry element to relate two chiral helices is only horizontal 2-fold screw axes. Therefore, the space group $P2_12_12_1$ and its statistically disordered one are unique candidates. If these possibilities were totally denied, we will have to explore monoclinic or triclinic structures. Recently, Alemán et al.[12] have proposed the antiparallel arrangement of s(10/7) helices in the $P2_12_12_1$ unit cell by packing energy calculations, electron diffraction, and some simulations. In the present work, the wide-angle X-ray diffraction (WAXD) data of the α-form were collected carefully, and the classical crystal structure analysis was performed.

Experimental Section

Materials. Samples of PLLA were provided by Dr. M. Sumita, Tokyo Institute of Technology, and Dr. T. Furukawa, Tokyo University of Science. The sample with the viscosity-average molecular weight 1.5×10^5 (intrinsic viscosity $[\eta] = 2.47$dL/g in chloroform at 25 °C[4]) was spun from the melt, which was conditioned on a hot plate at 190 °C. The crystallinity index was estimated to be about 30% by the Ruland procedure. By the subsequent heat treatment in hot water at 90 °C for 12 h, the crystallinity was much improved up to about 60% (comparable to that of high-density polyethylene), probably as a result of chain rearrangements induced by partial degradation and disentanglements on the lamella surface.

X-ray Diffraction. WAXD measurements were performed by using graphite-monochromatized Cu Kα radiation focused through a 0.3 mm pinhole collimator with the normal incidence to a flat 0.2×0.2 m^2 imaging plate (IP) detector of 1900×1900 pixels (R-AXIS IIc, Rigaku Corp.). The patterns were taken for the sample with the fiber axis being perpendicular (vertical) to the incident beam and also for the variously tilted ones in order to record the meridional reflections. The diffractograms were collected with the sample−IP distances $R_0 = 7$, 12, 16, and 20 cm and the exposure times 10, 20, 40, and 60 min. In the data files, 2 bytes was allotted to save each pixel intensity, and by the bit-shift storage technique the maximum recording intensity was 8 × 7FFF (hexadecimal) = 262 136 in the range of the linear sensitivity. In the patterns taken with short R_0 distance and long exposure time to seek weak reflections, the data of some strong reflections were overflowed and therefore omitted from the data collection.

By taking into account the effects of the distance from the sample to each pixel and the oblique incidence of the diffracted light onto IP, the crude intensity profile on IP can be transformed into the correct profile $I(\mathbf{q})$ to be measured with a conventional powder diffractometer:

$$I_{IP}(\mathbf{r}) \sim I(\mathbf{q}) \cos^3 2\theta / {R_0}^2 \quad (1)$$

where $|\mathbf{r}| = R_0 \tan 2\theta$ corresponds to the distance from the center of IP to the pixel, $\mathbf{q}$ is the scattering vector ($|\mathbf{q}| = 2 \sin \theta/\lambda$), 2θ is the diffraction angle, and λ is the X-ray wavelength. Here, we define an orthogonal coordinate system (u, v) on the IP pattern so that the v axis coincides with the projection of the fiber axis onto IP. Since the pattern is symmetrical with respect to the v line, the (u, v) axes are explicitly defined. Since the integral element is given by $\mathrm{d}u\ \mathrm{d}v = (R_0^2/\cos^3 2\theta)\ \mathrm{d}\Omega$

$$\int I_{IP}(\mathbf{r})\ \mathrm{d}u\ \mathrm{d}v = \int I(\mathbf{q})\ \mathrm{d}\Omega \quad (2)$$

where $\mathrm{d}\Omega$ is the solid-angle element. As a principle of energy conservation, the total intensity integrated over the area of an independent reflection is not altered with R_0 and the obliquity of IP. Actually, slight intensity decrease with R_0 was observed, owing to the air scattering in a manner of $I = I_0 \exp(-\mu_a R_0) \approx I_0(1 - \mu_a R_0)$, where μ_a is the mass absorption coefficient of air. These characteristics of IP have been confirmed by using standard samples for variously distant and oblique settings of IP.

The diffraction geometry for fibers has been well established.[21−25] The fiber-axis direction is specified by an angle μ of inclination of the fiber axis from the plane normal to the incident beam and a rotation angle β about the incident beam. The latter is the angle between the v axis and the vertical scanning axis of IP. These setting angles were reconfirmed from the quadruplet reflection positions. The inclination angle μ is an important parameter for Lorentz correction as is described below.

The integral intensities of the reflections were extracted in the following procedure. Independent spots on IP were enveloped with a quadrilateral or a fan-shaped region (defined by two concentric circles and two radial lines), and the pixel intensities in the region were numerically integrated over the background intensity surface that was approximated by the two-dimensional quadratic function optimized for the values along the envelope boundaries. Partly overlapping spots were similarly treated and separated by two-dimensional Gaussian curve fitting with respect to $\mathbf{r}$ and β. Peak profiles were not exactly Gaussian, but the fitting evaluations were fairly good compared to numerical integrations. Furthermore, the data on the layer-line traces were integrated and transformed into the profile with respect to ξ (radial coordinate of the cylindrical coordinate system in the reciprocal $\lambda\mathbf{q}$ space), and the peaks were separated by curve fitting. The center trace of the lth layer line is given by[21−24]

$$(v \cos \mu - R_0 \sin \mu)/({R_0}^2 + u^2 + v^2)^{1/2} + \sin \mu = l\lambda/c \equiv \zeta \quad (3)$$

The reflection coordinates (ξ, ζ) and d-spacings were calculated for the centers of gravity of the peak profiles by using geometrical equations following relationships $\xi^2 + \zeta^2 = |\lambda\mathbf{q}|^2 = (2 \sin \theta)^2 = (\lambda/d)^2$.

The intensity data were further corrected for Lorentz and polarization factors. The latter is the factor derived from the geometrical consideration.[26] The Lorentz correction gives the intensity integrated in the reciprocal space, and therefore yields the structure amplitude, from the observed intensity integrated for a spot on diagram. For uniaxial symmetry, the Lorentz factor L relates the integral elements in both spaces by a relationship $2\pi\xi\ \mathrm{d}\xi\ \mathrm{d}\zeta = 2\pi L^{-1}\ \mathrm{d}\Omega$ and is given by

$$L^{-2} = \sin^2 2\theta - \zeta^2 + 4 \sin^2 \theta \sin \mu\ (\zeta - \sin \mu) \quad (4)$$

as a modified expression for single-crystal rotation.[21−24] Arnott derived this equation on the basis of geometrical considerations.[21] Off-meridional small spots are satisfactorily integrated by multiplying L^{-1} of the center of gravity to the sum of pixel intensities. For near-meridional spots, it is better to carry out the integration by summation after multiplying L^{-1} to the intensity for each pixel. For the solitary meridional spot observed for the sample tilted by an angle $\mu = \sin^{-1}(\zeta/2)$, the integration is properly done by summation after multiplying $L^{-1}/2$ to each pixel intensity. Owing to the small L^{-1} values, even strong meridional reflections assume small structure amplitudes. With the normal-beam method ($\mu = 0$), the meridional spots are to be hidden in the so-called blind region. Generally, the meridional data observed for tilted samples have qualitatively been referred but often omitted from the quantitative analysis. This is because the meridional line has been regarded to be singular ($L^{-1} = 0$). However, the positions with zero L^{-1} correspond only to the center points in the $2\pi\xi\ \mathrm{d}\xi$ integral element. For a small meridional spot, the error of integration becomes large, and it may be recovered by eccentric rotation of the sample. Fortunately, this artificial disorientation was not necessary in the present work. The error in the intensity acquisition was about 5%; therefore, the error in structure amplitudes was less than 3%. The error was caused by the manner of envelopment of reflection, namely the evaluation of background scattering. The WAXD data of the α-form of PLLA were thus collected without the blind region

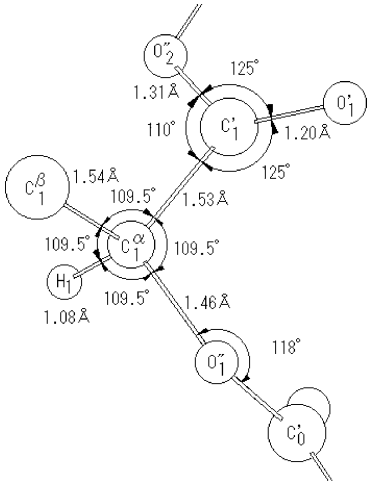

Figure 1. Molecular geometry of PLLA.

from a number of diagrams, and the structure amplitudes of 121 reflections were compared respectively and averaged after scaling. All the treatments of the IP data were carried out with PC computers.

Structure Analysis. Refinements of the crystal structure were performed by the linked-atom full-matrix least-squares method (LAFLS),[22,27] in which the bond lengths and bond angles can be constrained to their standard values. The linked-atom technique has been developed in order to cope with limited WAXD data for polymers and employed in many analyses.[18,22,27−32] Furthermore, this technique coupled with the Rietveld whole-fitting method[33] has been successfully applied to structure analyses.[35−37] The function minimized in the present analysis was Φ given by

$$\Phi = \sum_n (\sqrt{I_{o_n}} - \sqrt{I_{c_n}})^2 + \sum_h \lambda_h G_h \qquad (5)$$

where I_o's are observed intensities to be normalized by an adjustable scale factor, I_c's are the corresponding intensities calculated as mF^2 (or $\sum mF^2$ for overlapping reflections) (m = multiplicity, F = structure factor), and λ_h's are Lagrange multipliers for constraint relationships $G_h = 0$. In the structure-factor calculations, the hydrogen atoms of the methyl groups were neglected. The methyl groups are positioned with radius 2.8 Å farthest from the helical axis, while the remaining atoms are in the core region. Then, two isotropic temperature factors were assumed; $B_1 = 10$ Å^2 for the core atoms and $B_2 = 13$ Å^2 for the carbon atoms of the methyl groups. The LAFLS data included the 121 observed reflections as well as seven missing reflections assuming zero amplitudes. Results of the refinement cycles were evaluated by the discrepancy index $R = \sum(\sqrt{I_o} - \sqrt{I_c})/\sum\sqrt{I_o}$ for the 128 reflection data. If the structure model is essentially true, the refined atomic coordinates are little affected by the values of temperature factors, while the R index is certainly improved by the B factors. At the initial stage of refinements in some cases, the temperature factors are abnormally refined in order to reduce the R index, directing toward the false structure. Then the B values were fixed at this stage.

Our program starts the building of the molecular model with the standard dimensions (Figure 1).[5,12] Atomic notation is based on the IUPAC recommendation. Solving the Miyazawa equation[38] for the s(3*10/7) helix with $c = 28.88$ Å and the trans torsion angles of the ester bonds $\{\omega\} = \omega_1$ ($C^{\alpha}{}_1$, C'_1, O''_2, $C^{\alpha}{}_2$) = 180°, the skeletal torsion angles were calculated to be $\{\varphi\} = \varphi_1$ (C'_0, O''_1, $C^{\alpha}{}_1$, C'_1) = −66.0°, and $\{\psi\} = \psi_1$ (O''_1, $C^{\alpha}{}_1$, C'_1, O''_2) = 150.8°, as was reported previously. For computational simplicity, an ester oxygen atom (O''_1) carrying no pendant atom was chosen as the origin.

Energy Calculations. To examine the LAFLS results, conformational and packing energies were evaluated by using the hybrid force field developed by Weiner et al.,[39,40] where some kinds of atomic groups were treated as united atoms. In the present work, the methyl groups were regarded as single spheres, whereas the remaining atoms were explicitly included as was done by Alemán et al.[12] Nonbonded interactions (NB) were computed by a Lennard-Jones 6−12 potential without the 1−4 scale factor (for atom pairs separated by three bonds).[39−41] The results were comparatively insensitive to the 1−4 scaling. Electrostatic interactions (EL) were evaluated as Coulombic terms with a dielectric constant of 2.0. Torsional contributions (TW) were calculated only for torsions of ester bonds (ω) with a 2-fold rotational barrier of 8.0 kcal/mol.[41] The intrachain energy of the s(3*10/7) helix was $E_0 = 1.3$ (NB) + 2.7 (EL) = 4.0 kcal/mol for one repeat unit (10 monomeric residues).

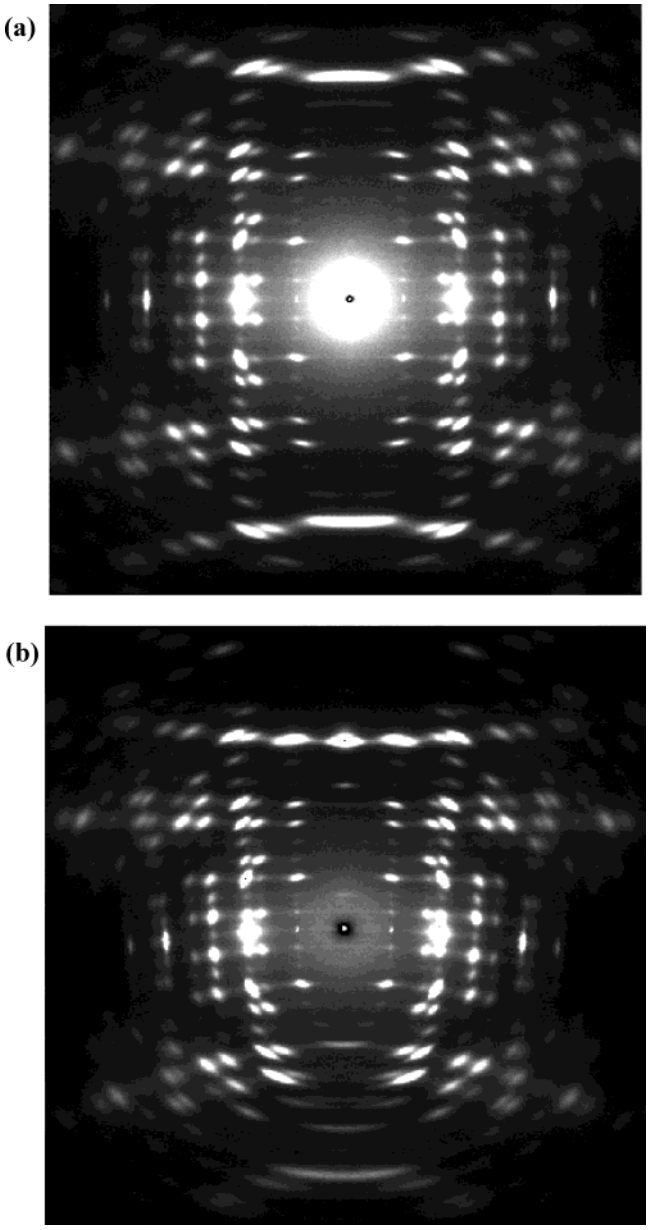

Figure 2. WAXD patterns of the α-form of PLLA: (a) vertical sample ($\mu = 0°$); (b) tilted sample ($\mu = 15.5°$) to observe the meridional spot on the tenth layer line.

Results and Discussion

Unit Cell. The X-ray fiber diagrams of the α-form of PLLA were identical to those reported by Hoogsteen et al.[5] Typical ones are shown in Figure 2. The well-arranged reflections were indexed with an orthorhombic unit cell containing two chains. The lattice parameters

were determined by the least-squares refinements for the reciprocal values of the observed *d*-spacings; a = 10.66(1) Å, b = 6.16(1) Å, and c (chain axis) = 28.88(2) Å. The crystal density is 1.26 g/cm^3. The cell dimensions are in the scope of the reported values that were dispersed in the intervals $\Delta a \approx \Delta b \approx 0.4$ Å and $\Delta c \approx 1$ Å. In addition to the diffraction spots, weak streaks were observed on the layer lines. These indicate some disorder in the axial translation and/or in arrangements of chain directions.

For a series of tilted samples, meridional reflections were observed on the layer lines with l = 2, 4, 6, 7, 8, and 10. The 007 reflection was neglected in the present analysis, since it was very weak and looked actually like a part of streak. Other unexpected spots were identified to be $\lambda/2$ diffractions of strong reflections by the measurements with the different high voltages of the X-ray generator. For instance, the apparent 100 spot was false one from (200) planes, and a spot observed between the first and second layer lines was also false one from (203) planes. The essential systematic absences were consistent with the space group $P2_12_12_1$.

Primary Structure. The $P2_12_12_1$ structure was first examined with the regular s(3*10/7) helix. As a cell definition, the $2_1(c)$ axis was placed at the corner so that the unit cell contains one chain in the center and four chains at the four corners, and the $2_1(a)$ axes were laid on (001) plane at z = 0. The general point coordinates are (x, y, z), ($-x$, $-y$, $z+1/2$), ($x+1/2$, $-y+1/2$, $-z$), and ($-x+1/2$, $y+1/2$, $-z+1/2$). The position of the parent chain at the (0, 0) corner is to be defined by the cylindrical coordinates of O″$_1$ atom chosen as the origin, namely, the setting angle τ(O″$_1$) (to the *ac* plane), and the axial fractional coordinate z(O″$_1$). Because of the regular helical symmetry, it is not necessary to survey the region of τ(O″$_1$) = 0−360° and z(O″$_1$) = 0−1.0. Since the second monomeric unit exists by the displacement Δz = 0.1, the scope of z(O″$_1$) = 0−0.1 is enough to survey the crystal structure models. Furthermore, the structure with rotational displacement $\Delta\tau$ = 180° is equivalent to the original model since τ(O″$_6$) = τ(O″$_1$) + 180°. Therefore, the independent region is covered by τ(O″$_1$) = 0−180° and z(O″$_1$) = 0−0.1 as was confirmed by the structure-factor calculations.

Structure factors and the R indices were calculated with steps $\Delta\tau$(O″$_1$) = 10° and Δz(O″$_1$) = 0.01. In Figure 3a, two distinct minima with R = 37% are observed. I: τ(O″$_1$) = 92° and z(O″$_1$) = 0.05; II: τ(O″$_1$) = 147° and z(O″$_1$) = 0.00. In the corresponding structures of I and II, the setting angles for C$^\alpha$ are τ(C$^\alpha_0$) = 160° and τ(C$^\alpha_4$) = 143°, respectively, although it was postulated to be τ(C$^\alpha$) = 150° by Alemán et al.[12] Since τ(O″$_2$) = 39° and z(O″$_2$) = 0.10 in model II, the minimum II is equivalent to II′.

Packing energies (NB and EL interactions), namely, E_1 between neighboring parallel chains (separated by a distance a) and E_2 between neighboring antiparallel (center and corner) chains, were evaluated with the same grid steps for one repeat unit (10 monomeric residues). The energies (E_1 + $2E_2$) for I and II were −34.5 and −34.2 kcal/mol, respectively. The total energies E_0 + E_1 + $2E_2$ are plotted in Figure 3b. The structures I and II are evenly matched at this stage.

Refinements. The LAFLS refinements were carried out by taking into account the chain distortion. In the first place, the (φ, ψ) torsion angles were adjusted by keeping the ω angles at 180°. The refined parameters

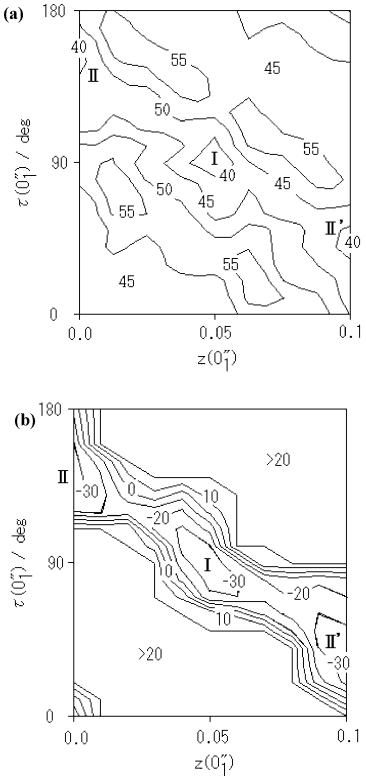

Figure 3. Plots of discrepancy index R (%) (a) and potential energy (b) as functions of axial displacement and the setting angle of the s(3*10/7) parent helix at the corner of $P2_12_12_1$ unit cell. The energy is expressed in kcal/mol for one repeat unit (10 monomeric residues). The contours are at intervals of 10 kcal/mol.

are τ(O″$_1$) and z(O″$_1$) designating the chain position as a whole, five sets of (φ, ψ) angles for an asymmetric unit, and a scale factor for the structure amplitudes. Since the chain repeating condition provides two G_h constraint conditions, the degree of freedom for the adjustable parameters is 11.

Starting at various chain positions, the LAFLS cycles were converged to two kinds of structures, I′ (R = 23%) and II′ (R = 30%), in which the chains were distorted periodically from s(3*10/7) in the packing models I and II, respectively. Structure I′ was considered to be valid, but the R index could not be further improved. Then, all the torsion angles as well as the ω angles were refined, where the 18 parameters with two constraints are still sufficiently small in number in comparison with the reflection data. After the cycles starting from I and II, the R indices were fairly improved respectively; I″: 12% and II″: 25%. The structure I″ was supported by the potential energies (in kcal/mol) E_0 = 2.4(NB) + 2.7(EL) + 2.6(TW) = 7.7 and E_1 = E_2 = −13.1, while structure II″ was clearly unfavorable for E_0 = 4.0(NB) + 2.7(EL) + 5.4(TW) = 12.1, E_1 = −11.1, and E_2 = −10.7. The energy difference between I″ and II″ corresponds to 1.2 kcal/mol for one monomeric residue.

The helix distortion during the refinement procedure from I to I″ is illustrated in Figure 4. The difference in appearance is hardly discernible in the side views, while it is clearly observed in the projections along the chain axis.

The representation of the crystal structure was examined. The standard deviations of torsion angles derived from the diagonal terms of the inverse matrix of normal equation were about 2°, but they were not

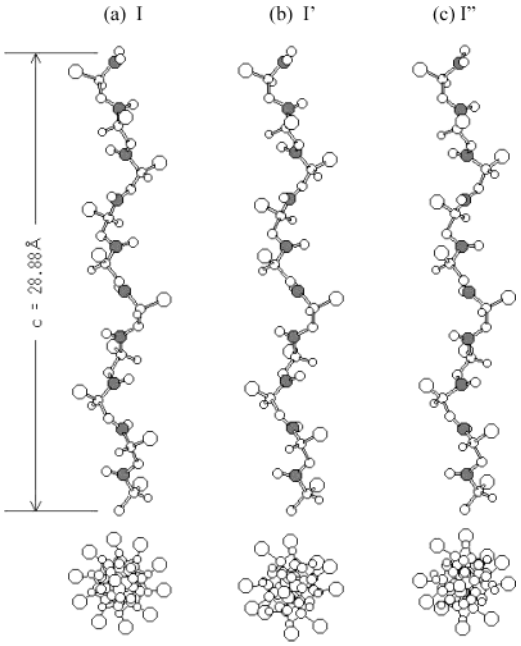

Figure 4. Helical structures in models I (a), I′ (b), and I″ (c). Shadowed circles denote the carbonyl carbon atoms, and the outer large circles denote the methyl groups. Lower: the projection along the chain axis.

directly interpreted as the analytical error. We prepared several data sets for the observed amplitudes within the 3% error and reiterated the above refinements. The *R* indices of the resultant structures were in the range 12−15%, and the manner of chain distortion was essentially the same. The variation in the final values of the torsion angles was mostly less than 2°, but the maximum difference was 4°. Therefore, the error in torsion angles was considered to be about ±2° at most. The error in orthogonal atomic coordinates was about 0.02 Å.

Next, the presumed values of bond lengths, bond angles, and temperature factors B_1 and B_2 were examined. A hasty increase of adjustable parameters may derive false local-minimum structures, as mentioned already. Then, refinements were reiterated with various preset values for these parameters, and the results were examined by the *R* index and the potential energies. The internal dimensions given in Figure 1 and the assumed B_1 and B_2 values were actually the best set. In the most probable final structure, $\tau(O''_1) = 86.8°$, $z(O''_1) = 0.057$, and the (φ, ψ, ω) angles (deg) for the five monomeric residues are 1 (−66.0, 163.9, 167.3), 2 (−63.0, 154.5, 165.0), 3 (−58.0, 150.0, 168.6), 4 (−65.8, 158.7, 178.1), and 5 (−68.2, 151.6, 175.4). The fractional atomic coordinates listed in Table 1 allow for the above-mentioned error. The structure is illustrated in Figure 5, and the observed and calculated intensities are compared in Figure 6.

Potential energies of the final structure I″ and the original model I were compared. The packing energy decreased by $\Delta(E_1 + 2E_2) = (-39.3) - (-34.5) = -4.8$ kcal/mol on the sacrifice of chain distortion $\Delta E_0 = 7.7 - 4.0 = 3.7$ kcal/mol. The energy difference between I and I″ is not so remarkable. The chain distortion results from a sort of uniform stress distribution.

In the crystal structure analysis of polymers, the *R* value of 20% is a criterion; false structures hardly give rise to the *R* value less than 20%. The value 12% for model I″ is fairly good and enough to believe the structure. Nevertheless, we examined the possibility for

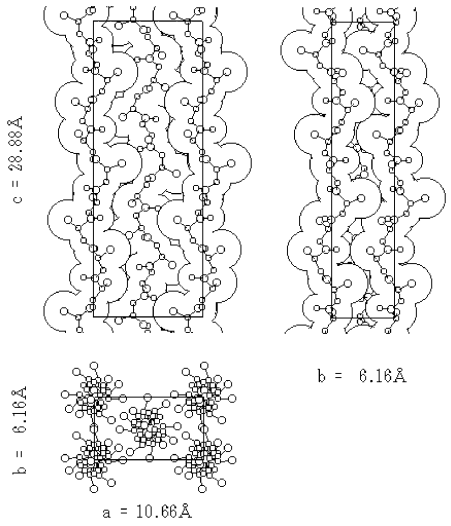

Figure 5. Crystal structure of the α-form of PLLA. Upper left: *ac* projection; upper right: *bc* projection, lower: *ab* projection. In the *ac* and *bc* projections, chains are enveloped with van der Waals radii of the constituent atoms.

Table 1. Atomic Fractional Coordinates of the Five Residues of a Parent Chain Placed at the Corner of the $P2_12_12_1$ Unit Cell

residue	species	*x*	*y*	*z*
1	O″	0.0036	0.1115	0.0569
	C^{α}	0.0891	0.0603	0.0948
	C^{β}	0.1350	0.2722	0.1175
	H	0.1686	−0.0290	0.0816
	C′	0.0206	−0.0776	0.1309
	O′	−0.0912	−0.0977	0.1335
2	O″	0.1018	−0.1705	0.1586
	C^{α}	0.0549	−0.2709	0.2010
	C^{β}	0.1641	−0.3802	0.2269
	H	−0.0149	−0.3914	0.1923
	C′	−0.0041	−0.0970	0.2319
	O′	0.0226	0.0922	0.2313
3	O″	−0.0881	−0.1851	0.2592
	C^{α}	−0.1321	−0.0589	0.2988
	C^{β}	−0.2262	−0.1948	0.3270
	H	−0.1774	0.0873	0.2867
	C′	−0.0204	0.0016	0.3295
	O′	0.0733	−0.1046	0.3337
4	O″	−0.0421	0.1863	0.3504
	C^{α}	0.0423	0.2510	0.3878
	C^{β}	0.0086	0.4817	0.4041
	H	0.1379	0.2489	0.3754
	C′	0.0291	0.0925	0.4283
	O′	−0.0600	−0.0222	0.4351
5	O″	0.1294	0.1005	0.4544
	C^{α}	0.1324	−0.0352	0.4959
	C^{β}	0.2643	−0.0269	0.5175
	H	0.1100	−0.2007	0.4867
	C′	0.0362	0.0486	0.5309
	O′	−0.0002	0.2326	0.5333

the statistical arrangement of up- and down-pointing chains which was discussed by Alemán et al.[12] In the process of crystallization, a pair of up chains may prefer for close neighboring of a down chain. The rapid process misarranges them at certain lattice points, and it will cause intricate disturbance to the lattice periodicity. As a result of X-ray interference, the structure is equivalent to the virtual arrangements of up and down chains at each site with half occupancy, respectively. A crystallographic approach is to add horizontal 2-fold axes to the lattice symmetry, although the misarranged up and down chains are not necessarily related by the crystallographic 2-fold axes. Anyhow, it will transform the $P2_12_12_1$ space group into $C222_1$ or $I2_12_12_1$. These models

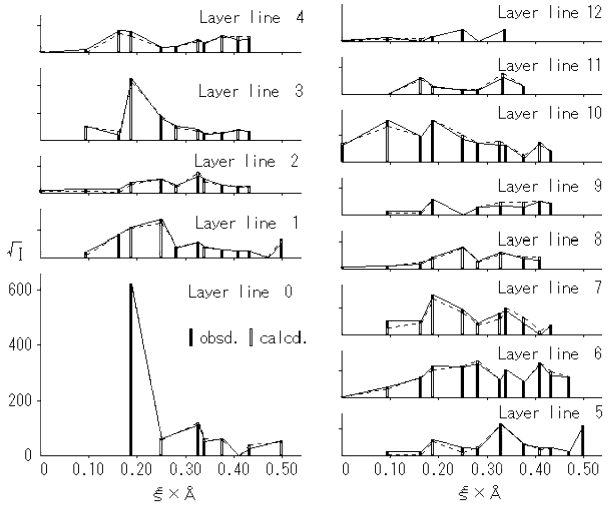

Figure 6. Comparison of I_o (connected by solid lines) and I_c (broken lines) for the fiber diffraction data of the α-form of PLLA.

are, however, denied because the systematic absences $h + k \neq 2n$ ($C222_1$) and $h + k + l \neq 2n$ ($I2_12_12_1$) are violated in the α-form. Replacements of the $2_1(a)$ and $2_1(b)$ axes in $P2_12_12_1$ by the 2-fold rotation axes yield $P222_1$, in which no symmetry element relates the chains at the centers and the corners. In this sense this space group is rather peculiar and not convincing. The number of refined parameters is to be doubled. Our LAFLS trials to search this type of statistical structure have failed.

Another plausible approach is based on a hypothesis that the misarranged up and down chains will possess the similar outer shape, namely, the similar locations of methyl groups that will contribute considerably to the interchain NB interactions. On the basis of the model I′ of $P2_12_12_1$, the antiparallel chains were added to respective lattice sites so that the methyl groups overlapped as close as possible. The refined parameters were $\tau(O''_1)$, $z(O''_1)$, and five sets of (φ, ψ, ω) angles for up and down chains and a scale factor for the structure amplitudes. The constraint conditions were two repeating conditions for up and down respective chains and five conditions for the overlapping of the methyl groups. The degree of freedom for the adjustable parameters was thus $35 - 9 = 26$. Even by this LAFLS refinement, the R index could not be decreased less than 36%. Without the constraint conditions for the overlapping of the methyl groups, the R index was decreased to 27%.

Consequently, the antiparallel chain arrangement is considered to be essential in the α-form and plays an important role in the polymorphism as in the case of isotactic polypropylene.

Acknowledgment. We thank Dr. M. Sumita and K. Inoue, Tokyo Institute of Technology, and Dr. T. Furukawa, Tokyo University of Science, for supplying poly(L-lactide) samples. We also thank Dr. T. Masuko, Yamagata University, for his valuable suggestions.

References and Notes

(1) Flory, P. J. *Statistical Mechanics of Chain Molecules*; John Wiley & Sons: New York, 1969.
(2) De Santis, P.; Kovacs, J. *Biopolymers* **1968**, *6*, 299.
(3) Kalb, B.; Pennings, A. J. *Polymer* **1980**, *21*, 607.
(4) Eling, B.; Gogolewski, S.; Pennings, A. J. *Polymer* **1982**, *23*, 1587.
(5) Hoogsteen, W.; Postema, A. R.; Pennings, A. J.; ten Brinke, G.; Zugenmaier, P. *Macromolecules* **1990**, *23*, 634.
(6) Kobayashi, J.; Asahi, T.; Ichiki, M.; Okikawa, A.; Suzuki, H.; Watanabe, T.; Fukada, E.; Shikinami, Y. *J. Appl. Phys.* **1995**, *77*, 2957.
(7) Miyata, T.; Masuko, T. *Polymer* **1997**, *38*, 4004.
(8) Cartier, L.; Okihara, T.; Lotz, B. *Macromolecules* **1997**, *30*, 6313.
(9) Cartier, L.; Okihara, T.; Ikada, Y.; Tsuji, H.; Puiggali, J.; Lotz, B. *Polymer* **2000**, *41*, 8909.
(10) Puiggali, J.; Ikada, Y.; Tsuji, H.; Cartier, L.; Okihara, T.; Lotz, B. *Polymer* **2000**, *41*, 8921.
(11) Kang, S.; Hsu, S. L.; Stidham, H. D.; Smith, P. B.; Leugers, M. A.; Yang, X. *Macromolecules* **2001**, *34*, 4542.
(12) Alemán, C.; Lotz, B.; Puiggali, J. *Macromolecules* **2001**, *34*, 4795.
(13) Okihara, T.; Tsuji, M.; Kawaguchi, A.; Katayama, K. *J. Macromol. Sci., Phys.* **1991**, *B30*, 119.
(14) Brizzolara, D.; Cantow, H.-J.; Diederichs, K.; Keller, E.; Domv, A. J. *Macromolecules* **1996**, *29*, 191.
(15) Allegra, G.; Corradini, P.; Elias, H.-G.; Geil, P. H.; Keith, H. D.; Wunderlich, B. *Pure Appl. Chem., Suppl.* **1989**, *61*, 769.
(16) *International Tables for Crystallography*; Hahn, T., Ed.; D. Reidel Pub. Co.: Dordrecht, 1983; Vol. A.
(17) Fraser, R. D. B.; MacRae, T. P. *Conformation in Fibrous Proteins*; Academic Press: New York, 1973.
(18) Takahashi, Y.; Tadokoro, H. *Macromolecules* **1973**, *6*, 672.
(19) Saruyama, Y.; Miyaji, H. *J. Polym. Sci., Polym. Phys. Ed.* **1985**, *23*, 1637.
(20) Saruyama, Y. *J. Phys. Soc. Jpn.* **1991**, *60*, 168.
(21) Arnott, S. *Polymer* **1965**, *6*, 478.
(22) French, A. D., Gardner, K. H., Eds. *Fiber Diffraction Methods*; ACS Symposium Series 141; American Chemical Society: Washington, DC, 1980.
(23) Fraser, R. D. B.; Suzuki, E.; MacRae, T. P. In *Structure of Crystalline Polymers*; Hall, I. H., Ed.; Elsevier: London, 1984; Chapter 1.
(24) Sasaki, S. *Rep. Prog. Polym. Phys. Jpn.* **1998**, *41*, 251.
(25) *International Tables for Crystallography*; Shmueli, U., Ed.; Kluwer: Dordrecht, 2001; Vol. B. *International Tables for Crystallography*; Wilson, A. J. C., Prince, E., Eds.; Kluwer: Dordrecht, 1999; Vol. C.
(26) Iannelli, P. *Macromolecules* **1993**, *26*, 2309.
(27) Arnott, S.; Wonacott, A. J. *Polymer* **1966**, *7*, 157; *J. Mol. Biol.* **1966**, *21*, 371.
(28) Sasaki, S.; Takahashi, Y.; Tadokoro, H. *J. Polym. Sci., Polym. Phys. Ed.* **1972**, *10*, 2363.
(29) Takahashi, Y.; Sato, T.; Tadokoro, H.; Tanaka, Y. *J. Polym. Sci., Polym. Phys. Ed.* **1973**, *11*, 233.
(30) Sasaki, S.; Iwanami, Y. *Macromolecules* **1988**, *21*, 3389.
(31) Millane, R. P.; Narasaiah, T. V. *Polymer.* **1989**, *60*, 1763.
(32) Inomata, K.; Sasaki, S. *J. Polym. Sci., Part B: Polym. Phys.* **1996**, *34*, 83.
(33) Rietveld, H. M. *J. Appl. Crystallogr.* **1969**, *2*, 65.
(34) Brückner, S.; Di Silvestro, G.; Porzio, W. *Macromolecules* **1986**, *19*, 235.
(35) Brückner, S.; Porzio, W. *Macromol. Chem.* **1988**, *189*, 961.
(36) Sasaki, S.; Yamamoto, T.; Kanbara, T.; Morita, A.; Yamamoto, T. *J. Polym. Sci., Part B: Polym. Phys.* **1992**, *30*, 293.
(37) Sasaki, S.; Maehara, K.; Nurulla, I.; Yamamoto, T. *Polym. J.* **2000**, *32*, 984.
(38) Miyazawa, T. *J. Polym. Sci.* **1961**, *55*, 215.
(39) Weiner, S. J.; Kollman, P. A.; Case, D. A.; Singh, U. C.; Ghio, C.; Alagona, G.; Profeta, S., Jr.; Weiner, P. *J. Am. Chem. Soc.* **1984**, *106*, 765.
(40) Weiner, S. J.; Kollman, P. A.; Nguyen, D. T.; Case, D. A. *J. Comput. Chem.* **1986**, *7*, 230.
(41) Wolf, R. M.; Francotte, E.; Glasser, L.; Simon, I.; Scheraga, H. A. *Macromolecules* **1992**, *25*, 709.

MA0348674